JOURNAL OF SYNCHROTRON RADIATION
ISSN 1600-5775

Demonstration of a picosecond Bragg switch for hard X-rays in a synchrotron-based pump–probe experiment

Mathias Sander,[a,b] Roman Bauer,[c,b] Victoria Kabanova,[a] Matteo Levantino,[a] Michael Wulff,[a] Daniel Pfuetzenreuter,[d] Jutta Schwarzkopf[d] and Peter Gaal[c,b]*

[a]European Sychrotron Radiation Facility, 71 Avenue des Martyrs, 38000 Grenoble, France, [b]Tailored X-ray Products gGmbH, Berlin, Germany, [c]Institut für Nanostruktur- und Festkörperphysik, Universität Hamburg, Luruper Chaussee 149, Hamburg 20355, Germany, and [d]Leibniz-Institut für Kristallzüchtung, Max-Born-Strasse 2, 12489 Berlin, Germany. *Correspondence e-mail: pgaal@physnet.uni-hamburg.de

Received 29 November 2018
Accepted 18 April 2019

Edited by G. Grübel, HASYLAB at DESY, Germany

Keywords: ultrafast X-ray diffraction; photoacoustics; synchrotrons; pump–probe experiments; active X-ray optics.

A benchmark experiment is reported that demonstrates the shortening of hard X-ray pulses in a synchrotron-based optical pump–X-ray probe measurement. The pulse-shortening device is a photoacoustic Bragg switch that reduces the temporal resolution of an incident X-ray pulse to approximately 7.5 ps. The Bragg switch is employed to monitor propagating sound waves in nanometer thin epitaxial films. From the experimental data, the pulse duration, diffraction efficiency and switching contrast of the device can be inferred. A detailed efficiency analysis shows that the switch can deliver up to 10^9 photons s^{-1} in high-repetition-rate synchrotron experiments.

1. Introduction

Currently, users in the synchrotron community with an interest in X-ray pulses of a sub-100 ps duration face a changing landscape of facilities. Conditions for time-resolved experiments have been improved significantly by the advent of X-ray free-electron lasers (XFELs), which provide ultrashort hard X-ray pulses of unprecedented brilliance [*Nature Photonics* editorial (2017), vol. 11, p. 609]. Alternatives for hard X-ray pulses of a few picoseconds or femtoseconds are the femto-slicing beamlines at the ALS (Schoenlein *et al.*, 2000) and SLS (Ingold *et al.*, 2007; Beaud *et al.*, 2007), table-top plasma sources (Zamponi *et al.*, 2009; Schick *et al.*, 2012) and the new FemtoMax facility at MAX IV (Enquist *et al.*, 2018). X-ray pulses with a duration of a few picoseconds are generated in third-generation storage rings using a low-charge-filling mode, the so-called low-α mode (Jankowiak & Wüstefeld, 2013). This mode reduces the total photon flux due to the low filling charge and is therefore only offered a few weeks per year. Currently, an upgrade project is planned for the BESSY II synchrotron (Helmholtz-Zentrum Berlin, 2015) which will provide a permanent improved low-α mode after the installation of additional RF cavities in the storage ring (Di Mitri, 2018).

In parallel with the commissioning of XFELs and alternative short-pulse sources, many existing synchrotrons are being updated to fourth-generation low-emittance storage rings (Schroer *et al.*, 2018). While low emittance provides better focusing properties and higher beam coherence, the temporal structure, *i.e.* the pulse duration and pulse repetition rate, is significantly less favourable for time-resolved experiments. Opportunities for time-resolved experiments at new

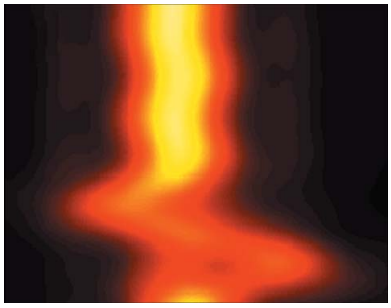

diffraction-limited synchrotron radiation facilities are discussed intensively within the community.

In this article we present a new photoacoustic Bragg switch that allows the shortening of hard X-ray pulses emitted from synchrotron storage rings, down to a few picoseconds. The idea of switching a synchrotron X-ray pulse with a controlled lattice deformation is almost 50 years old (Allam, 1970). Since then, several attempts have been made that relied on piezoelectric excitation (Grigoriev *et al.*, 2006; Zolotoyabko & Quintana, 2004), the generation of optical (Bucksbaum & Merlin, 1999; Sheppard *et al.*, 2005) and acoustic phonons (Gaal *et al.*, 2014; Sander *et al.*, 2016) or picosecond thermal excitations (Navirian *et al.*, 2011). Our device, which we call the PicoSwitch, has been tested in a synchrotron-based optical pump–X-ray probe experiment to measure the propagation of sound waves in epitaxial nanometer thin films. We discuss important quality parameters, *e.g.* the switching contrast and the angle- and time-dependent diffraction efficiency to determine the absolute pulse duration and photon efficiency of the shortened pulse. Based on our experimental results, we show that the switch can be operated at repetition rates of up to 1 MHz and delivers pulses of 5–10 ps duration. The device accepts a limited relative bandwidth of up to $\Delta E/E_0 = 0.2\%$. On the ID09 beamline at the European Synchrotron (ESRF), where our benchmark experiment was performed, the PicoSwitch can deliver a total flux of up to 10^9 photons s^{-1}, which is the typical intensity from a bending-magnet beamline at the ESRF.

2. Experimental

In the following, we give a brief introduction to the working principle of the PicoSwitch. A more comprehensive description can be found elsewhere (Sander *et al.*, 2016).

The layout of the pulse-shortening benchmark experiment is shown in Fig. 1(*a*). Unlike conventional pump–probe experiments, we employ two optical pump beams from the same laser source, one to trigger the PicoSwitch and the other to excite the sample. The time delay of the first excitation is selected such that the PicoSwitch diffracts incident photons while the maximum intensity of the long synchrotron X-ray pulse is present. Thus, only a temporal slice of the maximum intensity is diffracted from the PicoSwitch, while other parts of the X-ray pulse are suppressed. The shortened X-ray pulse impinges on the sample and is employed to probe dynamics induced by the second optical pump pulse. Since both the PicoSwitch and the sample are excited by optical pulses that stem from the same laser source, the time delay between the optical pump and the shortened X-ray probe pulse is completely jitter free. The relative pump–probe delay between the optical excitation of the sample and the shortened X-ray pulse is controlled by a motorized delay stage to record the transient sample dynamics up to a pump–probe delay of 2 ns.

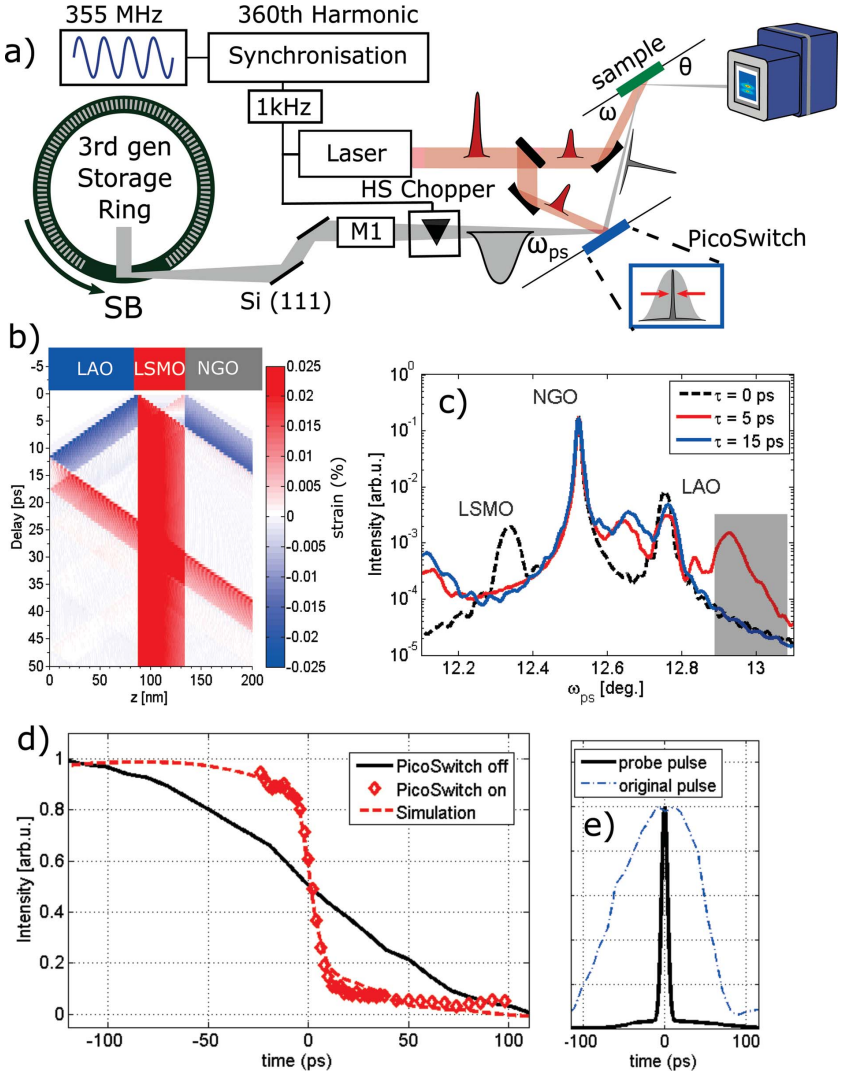

Figure 1
The working principle of the PicoSwitch. (*a*) The experimental setup on the ID09 beamline at the ESRF. Two optical pulses from a 1 kHz amplified laser system are employed to excite the PicoSwitch (blue) and the sample (green). X-ray pulses from the storage ring impinge on the PicoSwitch at an incidence angle ω_{ps}. A shortened X-ray pulse is diffracted to the sample at an incidence angle ω. (*b*) (Top) A sketch of the PicoSwitch and sample structure (details in the main text). The plot below shows a spatiotemporal strain map of propagating compression (red) and expansion (blue) waves in the bilayer structures. (*c*) Transient XRD curves of the PicoSwitch after laser excitation calculated from the strain map in panel (*b*). The simulations for 0 ps (black dashed line), 5 ps (red solid line) and 15 ps (blue solid line) show that the transient diffraction efficiency is turned on and off in the grey shaded area within a few picoseconds. (*d*) Pump–probe measurements with the shortened pulse (red symbols) and the original synchrotron pulse (black solid line) of the ultrafast decrease in diffraction efficiency from a nanostructure. A simulation of the short-pulse experiment is shown as a red dashed line. (*e*) The original (blue dot-dashed line) and shortened (black line) X-ray probe pulse. The original pulse was measured with a correlation technique (Gaal *et al.*, 2012) andthe shortened pulse was extracted from simulations (Gaal *et al.*, 2014; Sander *et al.*, 2016).

The PicoSwitch structure is shown in the top part of Fig. 1(*b*) and consists of two thin films grown by pulsed laser deposition (PLD) on a dielectric substrate (Sellmann *et al.*, 2014). The top layer is composed of a transparent dielectric. The bottom layer is an opaque metal that acts as a thermoelastic transducer upon optical excitation. We underline that several material combinations may be used to build a PicoSwitch device. Here, we use a combination of $LaAlO_3$ (LAO, 85 nm, transparent) and $La_{0.66}Sr_{0.33}MnO_3$ (LSMO, 57 nm, metallic) grown on an $NdGaO_3$ (NGO) substrate. Sound waves generated upon absorption of an optical pump pulse are shown in the coloured plot in Fig. 1(*b*) as expansive (red) and compressive (blue) strain. The strain pulses are launched from the interface of the transducer to the adjacent top layer and the substrate, respectively.

We calculate the impact of laser-generated strain waves on the angular diffraction efficiency of the PicoSwitch. The results are shown in Fig. 1(*c*) for pump–probe delays of 0, 5 and 15 ps (Schick *et al.*, 2014). The transient strain propagating through the PicoSwitch shifts the diffraction efficiency of the top LAO layer to larger diffraction angles and back to the initial position within 15 ps. The angular region is marked in grey in Fig. 1(*c*). Here, the PicoSwitch acts as a switchable mirror that is turned on and off by an acoustic pulse on a picosecond timescale.

An important quality parameter of the PicoSwitch is the switching contrast, which describes the suppression of incident X-ray photons during the off-state of the switch. The diffraction efficiency is at a low level η_0 before the arrival of the optical pump pulse. Upon laser excitation, the diffraction efficiency mounts to a high level η_{on} for a switching time ΔT, which is determined by the propagation of strain waves in the structure. After the coherent strain waves have propagated away from the thin films into the substrate, the diffraction efficiency falls back to its initial value $\eta_\infty \simeq \eta_0$. We define the switching contrast c_{sw} with the following expression (Gaal *et al.*, 2012),

$$c_{sw} = \frac{\eta - \eta_{0,\infty}}{\eta_{0,\infty}}. \quad (1)$$

c_{sw} basically has the same value before and after the switching is turned on and off This is a significant improvement compared to earlier designs of the PicoSwitch, where the final contrast $c_{sw,\infty}$ was strongly reduced by laser heating of the structure (Gaal *et al.*, 2014). Whether introducing the PicoSwitch results in high temporal resolution or not depends on the ratio of the pulse areas of the original and shortened pulses. Therefore, we define the total contrast c_{total} as the product of the switching contrast and the area loss factor, *i.e.* the ratio of the normalized pulse area of the original and shortened pulses,

$$c_{total} = c_{sw} \times \mathrm{ALF}, \quad (2)$$

where ALF is the area loss factor,

$$\mathrm{ALF} = \frac{\int_{-\infty}^{\infty} \mathrm{d}t\, I_{sw}(t) / I_{sw,m}}{\int_{-\infty}^{\infty} \mathrm{d}t\, \tilde{I}(t) / \tilde{I}_m}, \quad (3)$$

and $I_{sw}(t)$, $I_{sw,m}$, $\tilde{I}(t)$ and $\tilde{I}_m$ denote the time-dependent and maximum intensities of the shortened and original X-ray pulses, respectively. While $\tilde{I}(t)$ can be easily measured with the PicoSwitch (Gaal *et al.*, 2012), I_{sw} is deduced from model calculations as shown below.

The pulse-shortening capability is shown in Fig. 1(*d*), which shows a step-like decrease in the diffraction efficiency upon optical excitation. The sample and the physical origin of the sudden intensity change are discussed below. For now, we highlight the influence of the duration of the probe pulse on the measured dynamics. Fig. 1(*d*) clearly shows a dramatic increase in the temporal resolution of a measurement that employs the PicoSwitch. The temporal shape of the corresponding probe pulse is shown in Fig. 1(*e*). The original long synchrotron pulse was measured using a fast sampling method (Gaal *et al.*, 2012), which yields a full width at half-maximum (FWHM) pulse duration of 120 ps. We also clearly recognize the expected asymmetric pulse shape. The shortened pulse was derived from a simulation [red dashed line in Fig. 1(*d*)] and cross-checked by comparison with the experimental data.

3. Results and discussion

Now we discuss the experimental capabilities of the PicoSwitch pulse-shortening scheme in a real synchrotron-based pump–probe experiment. The sample is composed of a similar structure to the PicoSwitch itself, *i.e.* a thin-film system composed of a transparent dielectric LAO top layer with a thickness of 104 nm on a metallic LSMO layer with a thickness of 93 nm. The stack is grown on an NGO substrate. Note that the film thicknesses of the sample and the PicoSwitch are different, which results in slightly different propagation times of the coherent sound wave through the respective structure.

The lattice dynamics measured by time-resolved X-ray diffraction (XRD) of the metallic LSMO and dielectric LAO layers are shown in Figs. 2(*a*) and 2(*b*), respectively. Experiments were performed at an X-ray photon energy of 14.85 keV on the (002) lattice planes in symmetric ω–2θ geometry.

Both the sample and the PicoSwitch were mounted on motorized *xyz* translation stages and on a motorized rotation circle with angular resolution better than 0.1 mrad for tuning the incidence angle of the X-ray beam. The size of the X-ray beam before and after symmetric diffraction from the PicoSwitch was approximately 40 µm × 60 µm. The acceptance angle of the PicoSwitch was 870 µrad at an angle of 12.9°, which is eight times larger than the full vertical divergence in the focus of the X-ray beam. At the sample position, approximately 150 mm after the PicoSwitch, we observed no changes in the X-ray beam footprint, divergence or stability. In our setup, the shortened beam is deflected upwards. Insertion of a multilayer mirror could be used to deflect the beam downwards, thus yielding a horizontal beam. The repetition rate of the X-ray beam is reduced to 1 kHz by a system of choppers (Cammarata *et al.*, 2009) to match the laser repetition frequency. The main purpose of the choppers is to reduce the heat load on the beamline optics from the intense X-ray

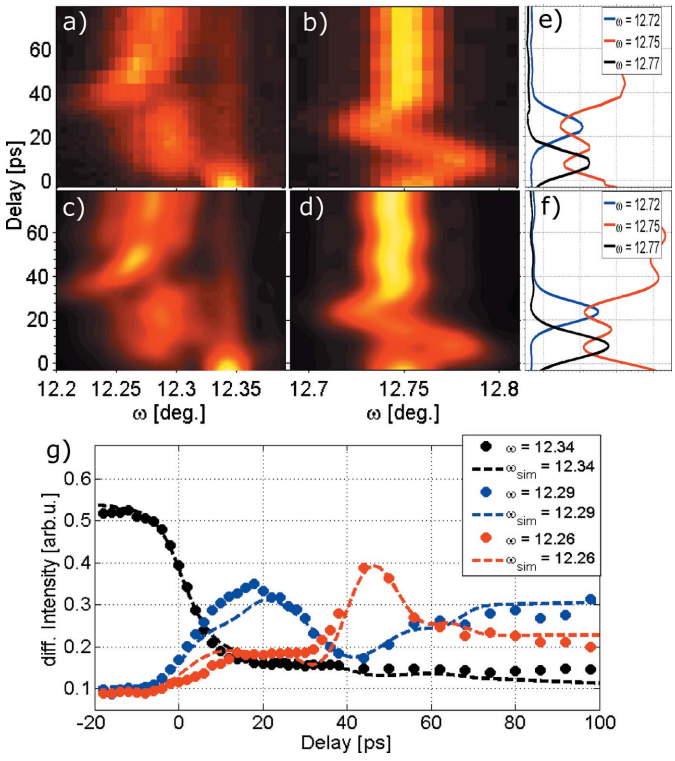

Figure 2
Experimental data. (*a*, *b*) Time-resolved measurements of propagating sound waves in (*a*) the LSMO film and (*b*) the LAO film of the sample. The measurement employed pulse shortening with the PicoSwitch. Fast picosecond lattice dynamics are clearly resolved by the experiment. The mechanism behind the observed XRD peak shift is outlined in the main text. (*c*, *d*) Simulations of propagating sound waves in (*c*) the LSMO layer and (*d*) the LAO layer. Comparison of the simulation and experimental data reveals an X-ray probe pulse duration of 7.5 ps and a total switching contrast of $c_{\rm total} = 2.94$. (*e*)–(*g*) Cross sections of measured and simulated data at different incidence angles ω on the sample.

radiation. They also protect soft-matter and biological samples from unnecessary radiation damage, thus leading to a longer sample lifetime. It should be noted that the PicoSwitch contrast is not sufficient to gate a single pulse from the synchrotron pulse train. Instead, gating can be performed electronically by modern detectors (Shayduk *et al.*, 2017). On the ID09 beamline, diffraction and scattering signals are recorded by a Rayonix HS170 detector in accumulation mode, *i.e.* the signal from many laser/X-ray pulse pairs is accumulated without any time resolution provided by the detector. Beam parameters are summarized in Table 1.

The sample and PicoSwitch were excited with an optical fluence of 30 mJ cm^{-2}. The principal axes of the elliptical laser footprint on the sample and PicoSwitch were 920 µm/600 µm and 720 µm/630 µm, respectively. We performed simulations of coherent acoustic phonon propagation in the sample using a one-dimensional linear chain model of masses and springs (Herzog, Schick *et al.*, 2012). The phenomenon of propagating high-frequency coherent acoustic phonon wavepackets is well understood (Thomsen *et al.*, 1986; Rose-Petruck *et al.*, 1999; Larsson *et al.*, 2002; Bargheer *et al.*, 2004; Bojahr *et al.*, 2013, 2015; Herzog, Bojahr *et al.*, 2012; Shayduk *et al.*, 2013). Our simulations yield a two-dimensional map of lattice strain

Table 1
Main parameters of the ID09 beamline at ESRF.

The second column lists the parameters after the Extremely Brilliant Source (EBS) upgrade (FWHM values).

	ESRF	ESRF-EBS
Focus		
H (µm)	40	20
V (µm)	60	20
Divergence		
H (µrad)	860	53
V (µrad)	106	28
Photons per pulse (pink beam)	2.1×10^9	3.0×10^9
Pulse duration	<135 ps	<150 ps

versus pump–probe delay along the out-of-plane spatial axis in the sample, as shown in Fig. 1(*b*). From the spatiotemporal strain map we calculate transient XRD curves using dynamic diffraction theory (Schick *et al.*, 2014; Warren, 1990). Finally, we convolute the XRD simulation with the simulated X-ray probe pulse after reflection from the PicoSwitch. The FWHM pulse duration of the shortened pulse is approximately 7.5 ps and the pulse is shown in Fig. 1(*e*).

Figs. 2(*c*) and 2(*d*) show simulated dynamics of the LSMO and LAO diffraction peaks, respectively. To reproduce the experimental data in a simulated pump–probe experiment, we find a switching contrast of $c_{\rm sw} = 33$. With ALF = 11.34 we find a total contrast $c_{\rm total}$ of 2.93. Both experiment and simulation show the effect of insufficiently suppressed photons of the original long X-ray pulse, *e.g.* at the equilibrium angle of the LSMO peak of 12.34 in Figs. 2(*a*) and 2(*c*). Still, the picosecond dynamics of the propagating sound waves are clearly resolved in the measurement.

Comparing the coloured plots shown in Figs. 2(*a*) and 2(*c*) and those in Figs. 2(*b*) and 2(*d*), we find excellent agreement of the simulated pump–probe experiment with the experimental data. In particular, we observe a step-like drop in the LSMO peak intensity at $\omega = 12.34°$ [black dashed line and black filled circles, Fig. 2(*g*)]. A delay scan at this incidence angle is shown in Fig. 1(*d*) compared with a measurement of the same dynamics with the original ESRF X-ray probe pulse. The LSMO peak reappears at $\omega = 12.29°$ for approximately 15 ps [blue dashed line and blue filled circles, Fig. 2(*g*)]. This new peak position corresponds to thermal expansion resulting from the energy deposited by the absorbed optical excitation pulse. At a pump–probe delay of ∼40 ps, the LSMO peak is distorted again but returns to its intermediate expanded angular position [red dashed line and red filled circles, Fig. 2(*g*)].

The dynamic features observed at the LSMO peak are well understood by simulations of thermal expansion and coherent phonon generation and propagation (Herzog, Schick *et al.*, 2012). The initial shift of the LSMO reflex stems from thermal expansion, while the second peak distortion originates from the coherent sound wave that is reflected back at the sample surface (Sander *et al.*, 2016). Having determined the sample geometry by static XRD and ellipsometry measurements, we adjust the simulated dynamics via the sound velocity in LSMO

and LAO, respectively, to the experimental data. The result agrees well with values reported by other groups (Bogdanova *et al.*, 2003; Michael *et al.*, 1992). For comparison, a similar experiment reported earlier by our group gave 20% higher sound velocities due to insufficient temporal and angular resolution of our XRD setup (Sander *et al.*, 2016).

As depicted in Fig. 2(*a*), we also observe a significant broadening of the LSMO peak after optical excitation. Within the time delay covered in the experiment, thermal transport and heat equilibration do not lead to a significant equilibration of strain within the two layers. Hence, due to the high temporal resolution provided by the PicoSwitch and the high angular resolution provided by the synchrotron, the initial excitation profile directly after absorption of the laser pulse is resolved. The data yield an exponential decay of the strain in the excited LSMO layer with a decay constant of 55 nm^{-1}.

Finally, we discuss the photon flux in the shortened X-ray pulse to check the efficiency of the PicoSwitch. By comparing the integral pulse areas of the original and shortened pulses shown in Fig. 1(*e*), we find an area loss factor ALF = 11.34. The total intensity loss must also account for the finite diffraction η_{on} of 2×10^{-3}. We find a total efficiency of 1.8×10^{-4}. Our measurement was performed with the U17 undulator on ID09 at the ESRF, which delivers 2.1×10^{6} photons per pulse at an energy of E_0 = 14.85 keV, a bunch current of 5 mA and a relative bandwith of $\Delta E/E_0$ = 0.016%. With the above considerations, the photon flux reduces to 3.6×10^{2} photons per pulse.

The calculated initial, final and total contrasts are shown in Fig. 3(*a*) for a monochromatic X-ray pulse. The high-contrast region also determines a limit for the angular stability of the switch. For experiments which tolerate a higher relative bandwidth, the number of photons can be increased almost linearly with the relative bandwidth $\Delta E/E_0$. However, the switching contrast decreases if the relative bandwidth is too large.

The effect of a finite total contrast is demonstrated in Fig. 3(*b*), which again depicts the sampling of the LSMO peak (black dashed line) with a probe pulse of 7.5 ps FWHM and contrasts of 2.93 (red solid line) and 1.35 (blue solid line). The simulated probe pulses are shown in Fig. 3(*c*). Clearly, increasing the bandwidth of the X-ray probe pulse yields a higher photon flux, but it goes hand in hand with a reduced switching contrast. Therefore, the total contrast and intensity of the PicoSwitch probe pulse are related quantities, which allow for adaptation to specific experiments.

We would like to point out again that the PicoSwitch contrast is insufficient for pulse gating. For that, slower photoacoustic transient gratings with diffraction efficiencies of up to 33% may be used (Sander, Herzog *et al.*, 2017; Sander, Pudell *et al.*, 2017). Another parameter for optimizing the experiment and the X-ray flux is to increase the repetition frequency of the PicoSwitch. A successful implementation of the PicoSwitch at a repetition rate of 208 kHz has already been presented (Sander *et al.*, 2016) and operation even above 1 MHz has been tested successfully. Assuming the PicoSwitch is operated at the ESRF orbit frequency of 354 kHz, the

Table 2
Performance parameters of the X-ray beam on ID09, the shortened beam during the experiment and an optimized setting with increased bandwidth and repetition rate.

For the beam size and beam divergence we also list the beamline parameters after the Extremely Brilliant Source (EBS) upgrade.

Parameter	ID09 (ESRF)	PicoSwitch experiment	PicoSwitch optimized
Photons per pulse			
$\Delta E/E_0 = 10^{-4}$	2×10^{6}	3.6×10^{2}	
$\Delta E/E_0 = 10^{-2}$	2×10^{8}		3.6×10^{4}
Photons per second			
At 1 kHz	2×10^{9}	3.6×10^{5}	
At 100 kHz	2×10^{11}		3.6×10^{9}

experimentally derived parameters from the measurement shown in Fig. 2 yield a total X-ray flux of 1.2×10^{8} photons s^{-1}. The main performance parameters of the short-pulse beam are summarized in Table 2, which also provides values for an optimized beamline setting with increased bandwidth and increased repetition frequency. As discussed above, both parameters increase the X-ray flux in the shortened beam. In Table 3 we provide the pulse parameters for other synchrotron-based short-pulse facilities.

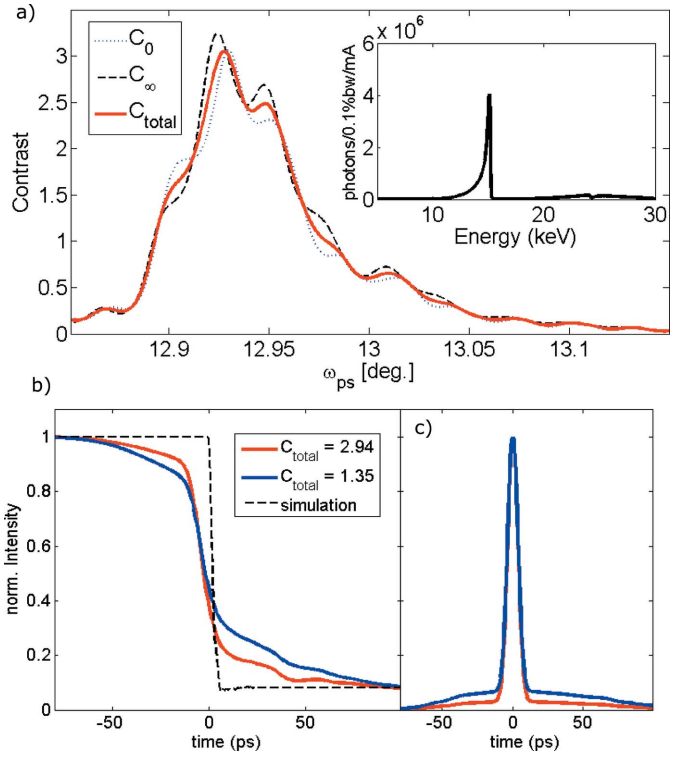

Figure 3
Switching contrast. (*a*) The calculated switching contrast of the PicoSwitch in the grey shaded area of Fig. 1(*c*). The contrast results from the difference in diffraction efficiency in the on and off states of the switch and from the area loss function ALF = 11.34. The inset shows the X-ray spectrum emitted by the U17 undulator on the ID09 beamline. (*b*) Calculated pump–probe signals of an ultrashort step function (black dashed line) with a contrast of 2.94 (red solid line) and 1.35 (blue solid line). The latter contrast is obtained at a ten times higher X-ray bandwidth. (*c*) X-ray probe pulses used for the calculations in panel (*b*).

Table 3
Summary of alternative synchrotron-based sources for picosecond and sub-picosecond X-ray pulses.

Parameter	FemtoMAX[a]	NSLS-II[b]	BESSY VSR[c]
Photons per pulse	1×10^7		
Energy (keV)	1.8–20	1–20	<10
Repetition rate	100 Hz	500 MHz	1.25 MHz
Pulse duration	100 fs	15–30 ps	15 ps to 300 fs

References: (*a*) Enquist *et al.* (2018); (*b*) NSLS-II, https://www.bnl.gov/ps/accelerator/; (*c*) Helmholtz-Zentrum Berlin (2015).

4. Conclusions

In conclusion, we have demonstrated the feasibility of pulse shortening with fast photoacoustic Bragg switches for synchrotron-based pump–probe experiments. Our device, which we call the PicoSwitch, shortens an incident 100 ps long hard X-ray pulse to a duration of 7.5 ps (FWHM). We have defined and quantified the relevant parameters for the pulse duration, efficiency and switching contrast of the PicoSwitch. Even with the rather low efficiency of a 1 kHz setup, our experiment monitors structural dynamics due to propagating sound waves in thin epitaxial films. In particular, we profit from the excellent beam stability and angular resolution of the synchrotron beam, which are not degraded by insertion of the PicoSwitch. In an optimized setup with repetition rates up to 1 MHz and a bandwidth of the X-ray pulse of 0.2%, the PicoSwitch would deliver a flux of more than 10^9 photons s^{-1}. The PicoSwitch is a powerful option for introducing high temporal resolution at the beamline level in synchrotron-based experiments. It may become a valuable tool for time-resolved experiments in current and future large-scale radiation facilities.

Funding information

Funding for this research was provided by: Bundesministerium für Bildung und Forschung (grant No. 05K16GU3); Horizon 2020 XPROBE (grant No. 637295 to Victoria Kabanova and Michael Wulff).

References

Allam, D. S. (1970). *J. Phys. E Sci. Instrum.* **3**, 1022–1023.
Bargheer, M., Zhavoronkov, N., Gritsai, Y., Woo, J. C., Kim, D. S., Woerner, M. & Elsaesser, T. (2004). *Science*, **306**, 1771–1773.
Beaud, P., Johnson, S. L., Streun, A., Abela, R., Abramsohn, D., Grolimund, D., Krasniqi, F., Schmidt, T., Schlott, V. & Ingold, G. (2007). *Phys. Rev. Lett.* **99**, 174801.
Bogdanova, K. G., Bulatov, A. R., Golenishchev-Kutuzov, V. A., Elokhina, L. V., Kapralov, A. V., Korolev, A. V., Neifel'd, A. & Shakirzyanov, M. M. (2003). *Phys. Solid State*, **45**, 298–303.
Bojahr, A., Gohlke, M., Leitenberger, W., Pudell, J., Reinhardt, M., von Reppert, A., Roessle, M., Sander, M., Gaal, P. & Bargheer, M. (2015). *Phys. Rev. Lett.* **115**, 195502.
Bojahr, A., Herzog, M., Mitzscherling, S., Maerten, L., Schick, D., Goldshteyn, J., Leitenberger, W., Shayduk, R., Gaal, P. & Bargheer, M. (2013). *Opt. Express*, **21**, 21188–21197.
Bucksbaum, P. H. & Merlin, R. (1999). *Solid State Commun.* **111**, 535–539.
Cammarata, M., Eybert, L., Ewald, F., Reichenbach, W., Wulff, M., Anfinrud, P., Schotte, F., Plech, A., Kong, Q., Lorenc, M., Lindenau, B., Räbiger, J. & Polachowski, S. (2009). *Rev. Sci. Instrum.* **80**, 015101.
Di Mitri, S. (2018). *J. Synchrotron Rad.* **25**, 1323–1334.
Enquist, H., Jurgilaitis, A., Jarnac, A., Bengtsson, Å. U. J., Burza, M., Curbis, F., Disch, C., Ekström, J. C., Harb, M., Isaksson, L., Kotur, M., Kroon, D., Lindau, F., Mansten, E., Nygaard, J., Persson, A. I. H., Pham, V. T., Rissi, M., Thorin, S., Tu, C.-M., Wallén, E., Wang, X., Werin, S. & Larsson, J. (2018). *J. Synchrotron Rad.* **25**, 570–579.
Gaal, P., Schick, D., Herzog, M., Bojahr, A., Shayduk, R., Goldshteyn, J., Leitenberger, W., Vrejoiu, I., Khakhulin, D., Wulff, M. & Bargheer, M. (2014). *J. Synchrotron Rad.* **21**, 380–385.
Gaal, P., Schick, D., Herzog, M., Bojahr, A., Shayduk, R., Goldshteyn, J., Navirian, H. A., Leitenberger, W., Vrejoiu, I., Khakhulin, D., Wulff, M. & Bargheer, M. (2012). *Appl. Phys. Lett.* **101**, 243106.
Grigoriev, A., Do, D.-H., Kim, D. M., Eom, C.-B., Evans, P. G., Adams, B. & Dufresne, E. M. (2006). *Appl. Phys. Lett.* **89**, 021109.
Helmholtz-Zentrum Berlin (2015). *Technical Design Study BESSY VSR.* https://www.helmholtz-Berlin.de/media/media/angebote/bibliothek/reports/r0001-bessy-vsr-tds.pdf.
Herzog, M., Bojahr, A., Goldshteyn, J., Leitenberger, W., Vrejoiu, I., Khakhulin, D., Wulff, M., Shayduk, R., Gaal, P. & Bargheer, M. (2012). *Appl. Phys. Lett.* **100**, 094101.
Herzog, M., Schick, D., Gaal, P., Shayduk, R., Korff Schmising, C. & Bargheer, M. (2012). *Appl. Phys. A*, **106**, 489–499.
Ingold, G., Beaud, P., Johnson, S., Streun, A., Schmidt, T., Abela, R., Al-Adwan, A., Abramsohn, D., Böge, M., Grolimund, D., Keller, A., Krasniqi, F., Rivkin, L., Rohrer, M., Schilcher, T., Schmidt, T., Schlott, V., Schulz, L., van der Veen, F. & Zimoch, D. (2007). *AIP Conf. Proc.* **879**, 1198–1201.
Jankowiak, A. & Wüstefeld, G. (2013). *Synchrotron Radiat. News*, **26**(3), 22–24.
Larsson, J., Allen, A., Bucksbaum, P., Falcone, R., Lindenberg, A., Naylor, G., Missalla, T., Reis, D., Scheidt, K., Sjogren, A., Sondhauss, P., Wulff, M. & Wark, J. S. (2002). *Appl. Phys. Mater. Sci. Process.* **75**, 467–478.
Michael, P. C., Trefny, J. U. & Yarar, B. (1992). *J. Appl. Phys.* **72**, 107–109.
Navirian, H. A., Herzog, M., Goldshteyn, J., Leitenberger, W., Vrejoiu, I., Khakhulin, D., Wulff, M., Shayduk, R., Gaal, P. & Bargheer, M. (2011). *J. Appl. Phys.* **109**, 126104.
Rose-Petruck, C., Jimenez, R., Guo, T., Cavalleri, A., Siders, C. W., Rksi, F., Squier, J. A., Walker, B. C. Wilson, K. R. & Barty, C. P. J. (1999). *Nature*, **398**, 310–312.
Sander, M., Herzog, M., Pudell, J. E., Bargheer, M., Weinkauf, N., Pedersen, M., Newby, G., Sellmann, J., Schwarzkopf, J., Besse, V., Temnov, V. V. & Gaal, P. (2017). *Phys. Rev. Lett.* **119**, 075901.
Sander, M., Koc, A., Kwamen, C. T., Michaels, H., v, A., Reppert, A., Pudell, J., Zamponi, F., Bargheer, M., Sellmann, J., Schwarzkopf, J. & Gaal, P. (2016). *J. Appl. Phys.* **120**, 193101.
Sander, M., Pudell, J.-E., Herzog, M., Bargheer, M., Bauer, R., Besse, V., Temnov, V. & Gaal, P. (2017). *Appl. Phys. Lett.* **111**, 261903.
Schick, D., Bojahr, A., Herzog, M., Shayduk, R., von Korff Schmising, C. & Bargheer, M. (2014). *Comput. Phys. Commun.* **185**, 651–660.
Schick, D., Bojahr, A., Herzog, M., von Korff Schmising, C., Shayduk, R., Leitenberger, W., Gaal, P. & Bargheer, M. (2012). *Rev. Sci. Instrum.* **83**, 025104.
Schoenlein, R. W., Chattopadhyay, S., Chong, H. H. W., Glover, T. E., Heimann, P. A., Shank, C. V., Zholents, A. A. & Zolotorev, M. S. (2000). *Science*, **287**, 2237–2240.
Schroer, C. G., Agapov, I., Brefeld, W., Brinkmann, R., Chae, Y.-C., Chao, H.-C., Eriksson, M., Keil, J., Nuel Gavaldà, X., Röhlsberger, R., Seeck, O. H., Sprung, M., Tischer, M., Wanzenberg, R. & Weckert, E. (2018). *J. Synchrotron Rad.* **25**, 1277–1290.

Sellmann, J., Schwarzkopf, J., Kwasniewski, A., Schmidbauer, M., Braun, D. & Duk, A. (2014). *Thin Solid Films*, **570**, 107–113.
Shayduk, R., Herzog, M., Bojahr, A., Schick, D., Gaal, P., Leitenberger, W., Navirian, H., Sander, M., Goldshteyn, J., Vrejoiu, I. & Bargheer, M. (2013). *Phys. Rev. B*, **87**, 184301.
Shayduk, R., Pennicard, D., Krausert, K., Gaal, P., Volkov, S., Vonk, V., Hejral, U., Jankowski, M., Reinhardt, M., Leitenberger, W. & Stierle, A. (2017). *J. Synchrotron Rad.* **24**, 1082–1085.
Sheppard, J. M. H., Sondhauss, P., Merlin, R., Bucksbaum, P., Lee, R. W. & Wark, J. S. (2005). *Solid State Commun.* **136**, 181–185.
Thomsen, C., Grahn, H. T., Maris, H. J. & Tauc, J. (1986). *Phys. Rev. B*, **34**, 4129–4138.
Warren, B. (1990). *X-ray Diffraction. Addison–Wesley Series in Metallurgy and Materials Engineering*. New York: Dover Publications.
Zamponi, F., Ansari, Z., Korff Schmising, C., Rothhardt, P., Zhavoronkov, N., Woerner, M., Elsaesser, T., Bargheer, M., Trobitzsch-Ryll, T. & Haschke, M. (2009). *Appl. Phys. A*, **96**, 51–58.
Zolotoyabko, E. & Quintana, J. P. (2004). *Rev. Sci. Instrum.* **75**, 699–708.